Non-uniform splitting of a single mantle plume by double cratonic roots: Insight into the origin of the central and southern East African Rift System

Alexander Koptev, Sierd Cloetingh, Taras Gerya, Eric Calais, Sylvie Leroy

1   **Non-uniform splitting of a single mantle plume by double cratonic roots:**

2   **Insight into the origin of the central and southern East African Rift System**

3   **Alexander Koptev[1,2], Sierd Cloetingh[3], Taras Gerya[4], Eric Calais[5], and Sylvie Leroy[1]**

4   [1]Sorbonne Universités, UPMC Univ Paris 06, CNRS, Institut des Sciences de la Terre de Paris

5   (iSTeP), 4 place Jussieu 75005 Paris, France

6   [2]Now at Department of Geosciences, University of Tübingen, Tübingen, Germany

7   [3]Department of Earth Sciences, Utrecht University, Netherlands

8   [4]ETH-Zurich, Institute of Geophysics, Sonnegstrasse 5, Zurich, Switzerland

9   [5]Ecole Normale Supérieure, Dept. of Geosciences, PSL Research University, CNRS UMR 8538,

10   Paris, France

11   Corresponding author: Alexander Koptev, Department of Geosciences, University of Tübingen,

12   Wilhelmstrasse 56, D-72074 Tübingen, Germany.

13   e-mail: alexander.koptev@ifg.uni-tuebingen.de.

14   Short title (running head): **Non-uniform splitting of a mantle plume by cratons**

15

Abstract

16

17   Using numerical thermo-mechanical experiments we analyze the role of active mantle

18   plume and pre-existing lithospheric thickness differences in the structural development of the

19   central and southern East African Rift system. The plume-lithosphere interaction model setup

20   captures the essential features of the studied area: two cratonic bodies embedded into surrounding

21   lithosphere of normal thickness. Results of numerical experiments suggest that localization of rift

22   branches in the crust is mainly defined by the initial position of the mantle plume relative to the

23   cratons. We demonstrate that development of the Eastern branch, the Western branch and the

24   Malawi rift can be the result of non-uniform splitting of the Kenyan plume that has been rising

25   underneath the southern part of the Tanzanian craton. Major features associated with Cenozoic

26   rifting can thus be reproduced in a relatively simple context of the interaction between a single

27   mantle plume and pre-stressed continental lithosphere with double cratonic roots.

28

Introduction

29

30   The East African Rift system (EARS) (McConnell, 1972; Chorowicz, 2005; Braile et al.,

31   2006; Ring, 2014) has two branches, the Eastern branch and Western branch. The N-S oriented

32   Eastern branch (Baker et al., 1972; Williams, 1982; Baker, 1987; Keller et al., 1991; Smith, 1994;

33   Mechie et al., 1997; Ebinger, 2005) extends over 2000 km from the Afar Triple Junction (Mohr,

34   1970; McClusky et al., 2003) in the north to the North Tanzanian Divergence Zone (Dawson,

35   1992; Le Gall et al., 2004, 2008; Isola et al., 2014) in the south (Figure 1) and consists of the

36   relatively narrow Main Ethiopian rift (Keranen et al., 2009), the wide rift in the Turkana

37   depression (Morley et al., 1992) and a narrow rift at the Tanzanian craton margin in the Kenya

38   rift (Zeyen et al., 1997). In the present study, however, we consider only the southern part of the

39   Eastern branch from Northern Kenya to North-Eastern Tanzania. The Western branch (Ebinger,

2

1989; Pasteels et al., 1989; Daly et al., 1989; Morley et al., 1999; Bauer et al., 2013) is composed

by the Albert-Edward, Kivu and Tanganyika-Rukwa rifts stretched in NE-SW, N-S and NW-SE

directions, respectively, depicting an arcuate map-trace along the western side of the Tanzanian

craton (Figure 1). The southern prolongation of the Western branch is represented by the Malawi

rift (Ring et al., 1992; Laó-Dávila et al., 2015) that is aligned on a N-S trend extending from the

Rungwe volcanic province (southern Tanzania) to the Urema graben (Mozambique). Geological

estimates indicate a higher degree of total lithospheric extension in the Kenya rift as compared to

the Western branch and the North Tanzanian Divergence Zone (Ring, 2014 and references

therein).

The Western and Eastern branches are separated by the Archaean (2500-3000 Ma)

Tanzanian craton (Bell and Dodson, 1981; Chesley et al., 1999; Manya, 2011) characterized by a

strong and cold lithosphere with a 150-300-km-thick keel (Artemieva, 2006; Adams et al., 2012;

Mulibo and Nyblade, 2013a,b). The 175-km-thick (Artemieva, 2006) Archaean-Paleoproterozoic

Bangweulu block (Andersen and Unrug, 1984; De Waele et al., 2006) that is stable since 1750

Ma (Lenoir et al., 1994), lies to the south-west of the Tanzanian craton. The Tanzanian and

Bangweulu cratons are both surrounded by Proterozoic orogenic belts (Cahen et al., 1984; Begg

et al., 2009) with a relatively thin (≤150 km) thermal lithosphere (Artemieva, 2006; Koptev and

Ershov, 2011).

Geophysical (e.g., Ritsema et al., 1998; Nyblade et al, 2000; Nolet et al., 2006) and

geochemical (e.g., Rooney et al., 2012; Armitage et al., 2015) observations indicate the presence

of mantle plumes under the EARS, possibly rooted into a common deep mantle anomaly

(Ritsema et al., 1999) corresponding to the African superplume. However, the actual number of

plumes and their relative position within this broad upwelling region remain contentious (e.g.,

Weeraratne et al., 2003; Chang and Van der Lee, 2011; Chang et al., 2015; Civiero et al., 2016).

64   It is commonly assumed that the Cenozoic rifts have avoided the cratons and follow the

65   mobile belts (McConnell, 1972; Mohr, 1982) which serve as the weakest pathways for rift

66   propagation. Structural control of the pre-existing heterogeneities within the Proterozoic belts at

67   the scale of individual faults or rifts has been demonstrated as well (Versfelt and Rosendahl,

68   1989; Ring, 1994; Theunissen et al., 1996; Corti et al., 2007; Morley, 2010; Katumwehe et al.,

69   2015; Smets et al., 2016).

70   However, as shown by Koptev et al. (2015, 2016), the formation of two rift zones on

71   opposite sides of a thick lithosphere segment can be explained without appealing to pre-imposed

72   heterogeneities at the crustal level. These models have provided a unified physical framework to

73   understand simultaneous development of the Western and Eastern branches around a thicker

74   Tanzanian craton (Roberts et al., 2012) as a result of the interaction between pre-stressed

75   continental lithosphere and single mantle plume anomaly corresponding to the Kenyan plume

76   (George et al., 1998; Pik et al., 2006; Chang and Van der Lee, 2011). Yet, the southern

77   prolongation of the Western rift by the Malawi rift has not been reproduced in any of these "one-

78   craton" experiments (Koptev et al., 2015, 2016). In order to overcome this discrepancy, we

79   follow-up on our previous studies with a series of laterally widened thermo-mechanical models

80   characterized by a presence of a second zone of lithospheric thickening that roughly mimics the

81   isometric (i.e. having equal horizontal dimensions) Bangweulu block situated south-west of the

82   Tanzanian craton and by a single mantle plume seeded underneath the southern part of the

83   Tanzanian craton (e.g., Hansen et al., 2012; Bagley and Nyblade, 2013).

84

85   **Model and experiments**

4

86   Our modeling is based on the thermo-mechanical viscous-plastic 3DELVIS code (Gerya

87   and Yuen, 2007) that combines the finite difference method with a marker-in-cell technique (see

88   Gerya (2010) for more details).

89   The 3D model box encompasses the entire 650-km-deep upper mantle, with large

90   horizontal scales (2000 × 2000 km) and offers "lithospheric-scale" resolution (~ 5 km × 5 km × 5

91   km per grid cell). The initial model setup corresponds to onset of a stratified three-layer

92   (upper/lower crust and lithospheric mantle) continental lithosphere which is underlain by

93   asthenospheric upper mantle. The initial geotherm is piece-wise linear, with 0°C at the surface,

94   700°C at the Moho, 1300°C at the lithosphere-asthenosphere boundary and 1630°C at the bottom

95   of the model box. The mantle plume is initiated by a temperature anomaly of +370°C at the base

96   of the upper mantle. In all presented experiments we have applied a constant extension in E-W

97   direction with a half rate of 3 mm/year, a typical value for pre-break-up continental rifts

98   including the Nubia-Somalia plate system (Stamps et al., 2008; Saria et al., 2014).

99   The general model series (Table 1; models **1**-**13**) is characterized by lateral homogeneity

100   of the crustal composition and by presence of two zones of 250 km-thick cratons embedded into

101   surrounding "normal" (150 km-thick) lithosphere. The first cratonic block is elongated in a N-S

102   direction (horizontal dimensions are 400 × 800 km) roughly mimicking the configuration of the

103   Tanzanian craton whereas the second one is small and isometric (horizontal dimensions are 400 ×

104   400 km) corresponding to the Bangweulu block. The initial plume location represents a key

105   controlling parameter of our study (Figure 2). In all performed experiments (except for "no-

106   plume" model **1**; Figure 3) the mantle plume has been shifted to the south up to 230 km with

107   respect to the center of the Tanzanian craton. We have studied the impact of small lateral

108   variations in its initial position: a southward shift varies from 210 km to 230 km whereas

109   latitudinal displacement is from 10 km to the west to 30 km to the east; different configurations

110   of the Tanzanian craton have been tested as well (Table 1; Figures 4-5). In order to investigate

111   the potential role of second-order structural heterogeneities we have performed several

112   complementary experiments (models **14**-**17**, Figure 6) including stronger (plagioclase flow law

113   instead of wet quartzite flow law) lower crust within the cratonic blocks (models **16**-**17**) and/or

114   third zone of lithospheric thickening situated to the west of the Tanzanian craton and roughly

115   mimicking the size and configuration of the Masai block (models **14**-**15**, **17**).

116

117   **Results and discussions**

118   Similarly to previous 3D experiments (Burov and Gerya, 2014; Koptev et al., 2015,

119   2016), the models presented here predict a rapid mantle ascent as the mantle plume reaches the

120   lithospheric bottom after 0.5 Myr. The common point of the performed models is a separation of

121   the upwelling plume head into three parts by the lithosphere of the Tanzanian and Bangweulu

122   blocks. After being divided, the buoyant plume material ponds at the base of "normal"

123   lithosphere adjacent to the western, eastern and southern sides of the Tanzanian craton (Figure 4).

124   In absence of active mantle upwelling ("no-plume" model **1**), ultra-slow tectonic

125   extension can only result in broadly distributed small-offset parallel faults (Figure 3). On the

126   contrary, in most of the other experiments (Figure 4), the continental crust above the hot plume

127   material is subjected to localized brittle deformation forming three linear, 100-500 km-long

128   rifting centers stretched in the direction perpendicular to external E-W extension. As already

129   shown by Burov and Gerya (2014), such large-scale linear normal faults are triggered and

130   maintained by mantle flow that impacts the bottom of continental lithosphere.

131   The degree of development (in terms of modeled strain rates) of each of these branches is

132   directly controlled by the relative amount of hot plume material ponding underneath the

133   corresponding lithosphere segment (Figure 4). In certain cases, however, this amount appears to

134   be too small to localize any visible deformation in the crust. For example, the plume's eastward

135   shift of 10 km in combination with the simplified shape of the Tanzanian craton results in the

136   absence of a discernible western rift (model **4**, Figure 4c). Similarly, the eastern branch is not

137   reproduced in the experiments assuming a more realistic Tanzanian craton and the mantle plume

138   with initial latitudinal displacement of 0 km or 10 km to the west (models **6** and **5**, respectively;

139   Figure 4e and Figure 4d). Only the plume's eastward shift up to 20 km (models **8**-**10**; Figure 4g-i)

140   can provide a symmetrical rifting on both (eastern and western) sides of the Tanzanian craton.

141   Further plume displacement to the east (up to 30 km) leads to a more developed eastern branch

142   comparing to the western one (models **11**-**13**; Figure 4j-l). The southern rift zone situated east of

143   the Bangweulu block is expressed clearly in all models. Note, however, that it becomes less

144   pronounced when the plume's southward shift decreases from 230 km to 210 km (compare

145   models **8** (Figure 4g) and **10** (Figure 4i) or models **11** (Figure 4j) and **13** (Figure 4l)). The

146   asymmetrical distribution of hot mantle material on the opposite sides of the craton (e.g., models

147   **11**-**12**) can provoke contrasted magmatic activity as observed in the central EARS, explaining a

148   magma-rich Eastern branch and magma-poor Western branch (e.g., Chorowicz et al., 2005; Ring,

149   2014).

150   We have identified model **9** (Figure 4h; Figure 5) as the "best-fit" experiment of the

151   general model series (models **1**-**13**) because it reproduces all three rift zones that are clearly

152   reflected not only in strain rate field but also in the surface topography (Figure 5c). Several other

153   models (such as models **3** or **8**), however, could also be considered as the "best-fit" (Figure 4b,g)

154   because they are able to reproduce a synchronous growth of the Eastern branch, the Western

155   branch and the Malawi rift as well. Note that modeled accumulated deformation in the localized

156   rift basins amounts to several tens km of total extension, that is in accord with geological

157   estimates for the central part of the EARS (e.g.. Ring, 2014 and references therein). A striking

158 feature is the consistency between modeled and observed rift distribution in case of the Kenyan

159 plume seeded underneath the southern part of the Tanzanian craton.

160   A principal shortcoming of this "best-fit" experiment (model **9**; Figure 5) is that it does

161 not reproduce the NW-SE oriented Rukwa rift segment of the Western branch (Figure 1).

162 Similarly to most of the other models, the southern end of the western branch penetrates into the

163 area underlain by the Bangweulu block. In this case, thick lithosphere appears to be not resistant

164 to lateral propagation of localized deformation given homogenous crustal composition adopted in

165 the general model series when crustal rheology of the cratonic blocks does not differ from

166 surrounding "normal" lithosphere. The situation changes completely when not only thicker

167 lithospheric mantle but also stronger rheology of the lower crust is considered for the cratonic

168 areas (complementary model series: models **16**-**17**, Figure 6c,d): in this case, localized strain

169 tends to avoid the strong cratons keeping them almost undeformed. In particular, this leads to the

170 change of orientation from N-S to NW-SE for the southernmost segment of the western branch

171 (corresponding to the Rukwa rift) thus providing a framework much more consistent with the

172 observed data. Introduction of the Masai block, for its part, improves the relative location of

173 widening of the rift zone in the southern segment of the eastern branch (models **15**, **17**; Figure

174 6b,d) that would correspond to the observed transition between the narrow Kenya rift to a

175 considerably wider zone (300-400 km) of block faulting in northern Tanzania (Dawson, 1992;

176 Ebinger et al., 1997; Foster et al., 1997; Le Gall, 2008; Corti et al., 2013).

177   It should be noted that given the better fit with the observed data in case of

178 complementary models containing more predefined complexities (see Figure 6d), the analyzed

179 plume-induced multi-branch continental rifting dynamics need further numerical investigation

180 and quantitative analysis of the controlling factors including complex 3D structure of the central

181   EARS in terms of inherited compositional and rheological heterogeneities of the crust and

182   lithospheric mantle (e.g., Sippel et al., 2017).

183

184   **Conclusions**

185   The fully-coupled thermo-mechanical models presented here start from relatively simple

186   initial conditions: a single mantle plume anomaly seeded underneath the continental lithosphere

187   embedding two cratonic blocks. These experiments evolve over time to create a complex system

188   characterized by asymmetrical splitting of the plume head into three parts. The resulting relative

189   distribution of hot plume material ponding below "normal" lithosphere is a controlling parameter

190   for deformation localization at the crustal level. Very small variations in initial plume position

191   with respect to cratonic bodies (up to several tens km only) appear to be able to change the

192   relation between these three segments of separated plume head that, in turn, alters the degree of

193   development of corresponding rift branches. We argue, thus, that the resulting rifting pattern is

194   largely controlled by relative position of the initial mantle plume anomaly with respect to first-

195   order lithospheric thickness differences rather than by second-order crustal and/or lithospheric

196   compositional heterogeneities as commonly assumed before (Theunissen et al., 1996; Corti et al.,

197   2007; Katumwehe et al., 2015; Smets et al., 2016).

198   The performed analysis permits to identify an initial model configuration that results in a

199   strain distribution that bears strong similarities with the central and southern EARS showing

200   simultaneous development of the Eastern branch, the Western branch and its southern

201   prolongation by the Malawi rift. The number and relative positions of rift branches with respect

202   to the cratons within the studied area can be explained by an impact of single mantle anomaly on

203   pre-stressed continental lithosphere that does not contain any pre-defined heterogeneities other

204   than the well-known cratonic blocks.

References

Adams, A., Nyblade, A. and Weeraratne, D., 2012. Upper mantle shear wave velocity structure beneath the East African plateau: evidence for a deep, plateauwide low velocity anomaly. *Geophysical Journal International*, **189**, 123-142.

Albaric, J., Déverchère, J., Petit, C., Perrot, J. and Le Gall B., 2009. Crustal rheology and depth distribution of earthquakes: insights from the central and southern East African Rift System. *Tectonophysics*, **468**, 28-41.

Andersen, L.S. and Unrug, R., 1984. Geodynamic evolution of the Bangweulu Block, northern Zambia. *Precambrian Research*, **25**, 187-212.

Armitage, J.J., Ferguson, D.J., Goes, S., Hammond, J.O.S., Calais, E., Rychert, C.A. and Harmon, N., 2015. Upper mantle temperature and the onset of extension and break-up in Afar, Africa. *Earth and Planetary Science Letters*, **418**, 78-90.

Artemieva, I.M., 2006. Global 1×1 thermal model TC1 for the continental lithosphere: implications for lithosphere secular evolution. *Tectonophysics*, **416**, 245-277.

228   Bagley, B. and Nyblade, A.A., 2013. Seismic anisotropy in eastern Africa, mantle flow, and the

229   African superplume. *Geophysical Research Letters,* **40***,* 1500-1505.

230   Baker, B.H., Mohr, P.A. and Williams, L.A.J., 1972. Geology of the eastern rift system of Africa.

231   *Geological Society of America Special Papers*, **136**, 1-68.

232   Baker, B.H., 1987. Outline of the petrology of the Kenya rift alkaline province. *Geological*

233   *Society, London, Special Publications*, **30**, 293-311.

234   Bauer, F.U., Glasmacher, U.A., Ring, U., Karl, M., Schumann, A. and Nagudi, B., 2013. Tracing

235   the exhumation history of the Rwenzori Mountains, Albertine Rift, Uganda, using low

236   temperature thermochronology. *Tectonophysics*, **599**, 8-28.

237   Begg, G.C. et al., 2009. The lithospheric architecture of Africa: Seismic tomography, mantle

238   petrology, and tectonic evolution. *Geosphere*, **5**, 23-50.

239   Bell, K. and Dodson, M.H., 1981. The geochronology of the Tanzanian Shield. *The Journal of*

240   *Geology*, **89**, 109-128.

241   Beniest, A., Koptev, A. and Burov, E., 2017a. Numerical models for continental break-up:

242   Implications for the South Atlantic. *Earth and Planetary Science Letters*, **461**, 176-189.

243   Beniest, A., Koptev, A., Leroy, S., Sassi, W. and Guichet, X., 2017b. Two- branch break- up

244   systems by a single mantle plume: Insights from numerical modeling. *Geophysical*

245   *Research Letters*, **44**.

246   Braile, L.W., Keller, G.R., Wendlandt, R.F., Morgan, P. and Khan, M.A., 2006. The East African

247   rift system. *Developments in Geotectonics*, **25**, 213-III.

248   Burov, E., 2011. Rheology and strength of the lithosphere. *Marine and Petroleum Geology*, **28**,

249   1402-1443.

250   Burov, E. and Cloetingh, S., 2010. Plume-like upper mantle instabilities drive subduction

251   initiation. *Geophysical Research Letters*, **37**.

252   Burov, E. and Gerya, T., 2014. Asymmetric three-dimensional topography over mantle plumes.
253   *Nature*, **513**, 85-89.

254   Burov, E. and Guillou-Frottier, L., 2005. The plume head–continental lithosphere interaction
255   using a tectonically realistic formulation for the lithosphere. *Geophysical Journal*
256   *International*, **161**, 469-490.

257   Burov, E., Guillou-Frottier, L., d'Acremont, E., Le Pourhiet, L. and Cloetingh, S., 2007. Plume
258   head-lithosphere interactions near intra-continental plate boundaries. *Tectonophysics*,
259   **434**, 15-38.

260   Cahen, L., Snelling, N., Delhal, J. and Vail, J., 1984. *The Geochronology and Evolution of*
261   *Africa.* Oxford Univ. Press, New York.

262   Chang, S.J. and Van der Lee, S., 2011. Mantle plumes and associated flow beneath Arabia and
263   East Africa. *Earth and Planetary Science Letters*, **302**, 448-454.

264   Chang, S.J., Ferreira, A.M.G., Ritsema, J., van Heijst, H.J. and Woodhouse, J.H., 2015. Joint
265   inversion for global isotropic and radially anisotropic mantle structure including crustal
266   thickness perturbations. *Journal of Geophysical Research: Solid Earth*, **120**, 4278-4300.

267   Chesley, J.T., Rudnick, R.L. and Lee, C.T., 1999. Re-Os systematics of mantle xenoliths from the
268   East African Rift: Age, structure, and history of the Tanzanian craton. *Geochimica et*
269   *Cosmochimica Acta*, **63**, 1203-1217.

270   Chorowicz, J., 2005. The east African rift system. *Journal of African Earth Sciences*, **43**, 379-
271   410.

272   Civiero, C.et al., 2016. Small-scale thermal upwellings under the northern East African Rift from
273   S travel time tomography. *Journal of Geophysical Research: Solid Earth*, **121**, 7395-
274   7408.

275 Corti, G., Iandelli, I. and Cerca, M., 2013. Experimental modeling of rifting at craton margins.

276   *Geosphere*, **9**, 138-154.

277 Corti, G., van Wijk, J., Cloetingh, S. and Morley, C.K., 2007. Tectonic inheritance and

278   continental rift architecture: Numerical and analogue models of the East African Rift

279   system. *Tectonics*, **26**.

280 Daly, M.C., Chorowicz, J. and Fairhead, J.D., 1989. Rift basin evolution in Africa: the influence

281   of reactivated steep basement shear zones. *Geological Society, London, Special*

282   *Publications*, **44**, 309-334.

283 Dawson, J., 1992. Neogene tectonics and volcanicity in the North Tanzania Sector of the Gregory

284   Rift Valley: Contrasts with the Kenya sector. *Tectonophysics*, **204**, 81-92.

285 De Waele, B., Liégeois, J.P., Nemchin, A.A. and Tembo, F., 2006. Isotopic and geochemical

286   evidence of Proterozoic episodic crustal reworking within the Irumide Belt of south-

287   central Africa, the southern metacratonic boundary of an Archaean Bangweulu Craton.

288   *Precambrian Research*, **148**, 225-256.

289 Ebinger, C., 2005. Continental break-up: the East African perspective. *Astronomy & Geophysics*,

290   **46**, 2-16.

291 Ebinger, C.J., 1989. Tectonic development of the western branch of the East African rift system.

292   *Geological Society of America Bulletin*, **101**, 885-903.

293 Ebinger, C., Poudjom, Y., Mbede, E., Foster, F. and Dawson, J., 1997. Rifting Archean

294   lithosphere: The Eyasi-Manyara-Natron rifts, East Africa. *Journal of the Geological*

295   *Society London*, **154**, 947-960.

296 Fishwick, S. and Bastow I.D., 2011. Towards a better understanding of African topography: a

297   review of passive-source seismic studies of the African crust and upper mantle.

298   *Geological Society, London, Special Publications*, **357**, 343-371.

299   Foster, A., Ebinger, C., Mbede, E. and Rex, D., 1997. Tectonic development of the northern

300   Tanzanian sector of the East African Rift System. *Journal of the Geological Society*

301   *London*, **154**, 689-700.

302   George, R., Rogers, N. and Kelley, S., 1998. Earliest magmatism in Ethiopia: evidence for two

303   mantle plumes in one flood basalt province. *Geology*, **26**, 923-926.

304   Gerya, T.V., 2010. *Introduction to Numerical Geodynamic Modelling*. Cambridge University

305   Press, 358 pp.

306   Gerya, T.V. and Yuen, D.A., 2007. Robust characteristics method for modelling multiphase

307   visco-elasto-plastic thermo-mechanical problems. *Physics of the Earth and Planetary*

308   *Interiors*, **163**, 83-105.

309   Hansen, S.E., Nyblade, A.A. and Benoit, M.H., 2012. Mantle structure beneath Africa and Arabia

310   from adaptively parameterized P-wave tomography: Implications for the origin of

311   Cenozoic Afro-Arabian tectonism. *Earth and Planetary Science Letters*, **319**, 23-34.

312   Huismans, R.S. and Beaumont, C., 2007. Roles of lithospheric strain softening and heterogeneity

313   in determining the geometry of rifts and continental margins. In: *Imaging, Mapping and*

314   *Modelling Continental Lithosphere Extension and Breakup* (Karner, G.D., Manatschal,

315   G.D., Pinheiro, L.M., eds). *Geological Society, London, Special Publications*, **282**, 111-

316   138.

317   Isola, I., Mazzarini, F., Bonini, M. and Corti, G., 2014. Spatial variability of volcanic features in

318   early-stage rift settings: the case of the Tanzania Divergence, East African rift system.

319   *Terra Nova*, **26**, 461-468.

320   Katumwehe, A.B, Abdelsalam, M.G. and Atekwana, E.A., 2015. The role of pre-existing

321   Precambrian structures in rift evolution: The Albertine and Rhino grabens, Uganda.

322   *Tectonophysics*, **646**, 117-129.

323   Keller, G.R., Khan, M.A., Morganc, P., Wendlandt, R.F., Baldridge, W.S., Olsen, K.H., Prodehl,

324   C. and Braile, L.W., 1991. A comparative study of the Rio Grande and Kenya rifts.

325   *Tectonophysics*, **197**, 355-371.

326   Keranen, K.M.*,* Klemperer, S.L.*,* Julia, J.*,* Lawrence, J.F. and Nyblade, A.A., 2009. Low lower

327   crustal velocity across Ethiopia: Is the Main Ethiopian Rift a narrow rift in a hot craton?

328   *Geochemistry Geophysics Geosystems,* **10***,* Q0AB01.

329   Koptev, A., Burov, E., Calais, E., Leroy, S., Gerya, T., Guillou-Frottier, L. and Cloetingh, S.,

330   2016. Contrasted continental rifting via plume-craton interaction: Applications to Central

331   East African Rift. *Geoscience Frontiers*, **7**, 221-236.

332   Koptev, A., Burov, E., Gerya, T., Le Pourhiet, L., Leroy, S., Calais, E. and Jolivet, L., 2017a.

333   Plume-induced continental rifting and break-up in ultra-slow extension context: Insights

334   from 3D numerical modeling. *Tectonophysics*, doi.org/10.1016/j.tecto.2017.03.025.

335   Koptev, A., Calais, E., Burov, E., Leroy, S. and Gerya, T., 2015. Dual continental rift systems

336   generated by plume-lithosphere interaction. *Nature Geoscience*, **8**, 388-392.

337   Koptev, A., Cloetingh, S., Burov, E., François, T. and Gerya, T., 2017b. Long-distance impact of

338   Iceland plume on Norway's rifted margin. *Scientific Reports*, **7**.

339   Koptev A.I. and Ershov A.V., 2011. Thermal thickness of the Earth's lithosphere: a numerical

340   model. *Moscow University Geology Bulletin*, **66**, 323-330.

341   Laó-Dávila, D.A., Al-Salmi, H.S., Abdelsalam, M.G. and Atekwana, E.A., 2015. Hierarchical

342   segmentation of the Malawi Rift: The influence of inherited lithospheric heterogeneity

343   and kinematics in the evolution of continental rifts. *Tectonics*, **34**, 2399-2417.

344   Le Gall, B., Gernigon, L., Rolet, J., Ebinger, C., Gloaguen, R., Nilsen, O., Dypvik, H.,

345   Deffontaines, B. and Mruma, A., 2004. Neogene-Holocene rift propagation in central

346   Tanzania: Morphostructural and aeromagnetic evidence from the Kilombero area.

347   *Geological Society of America Bulletin*, **116**, 490-510.

348 Le Gall, B., Nonnotte, P., Rolet, J., Benoit, M., Guillou, H., Mousseau-Nonnotte, M., Albaric, J.

349   and Deverchère, J., 2008. Rift propagation at craton margin: Distribution of faulting and

350   volcanism in the North Tanzanian Divergence (East Africa) during Neogene times.

351   *Tectonophysics*, **448**, 1-19.

352 Lenoir, J.L., Liégeois, J.P., Theunissen, K. and Klerkx, J., 1994. The Palaeoproterozoic Ubendian

353   shear belt in Tanzania: geochronology and structure. *Journal of African Earth Sciences*,

354   **19**, 169-184.

355 Manya, S., 2011. Nd-isotopic mapping of the Archaean–Proterozoic boundary in southwestern

356   Tanzania: Implication for the size of the Archaean Tanzania Craton. *Gondwana*

357   *Research*, **20**, 325-334.

358 McClusky, S., Reilinger, R., Mahmoud, S., Sari, D.B. and Tealeb, A., 2003. GPS constraints on

359   Africa (Nubia) and Arabia plate motions. *Geophysical Journal International*, **155**, 126-

360   138.

361 McConnell, R.B., 1972. Geological development of the rift system of eastern Africa. *Geological*

362   *Society of America Bulletin*, **83**, 2549-2572.

363 Mechie, J., Keller, G.R., Prodehl, C., Khan, M.A. and Gaciri, S.J., 1997. A model for the

364   structure, composition and evolution of the Kenya rift. *Tectonophysics*, **278**, 95-119.

365 Mohr, P., 1982. Musings on continental rifts. In: *Continental and oceanic rifts* (G. Palmason, ed).

366   *American Geophysical Union Geodynamics Series*, **8**, 293-309.

367 Mohr, P.A., 1970. The Afar Triple Junction and sea-floor spreading. *Journal of Geophysical*

368   *Research*, **75**, 7340-7352.

369 Morley, C.K., 2010. Stress re-orientation along zones of weak fabrics in rifts: An explanation for

370 pure extension in 'oblique' rift segments? *Earth and Planetary Science Letters*, **297**, 667-

371 673.

372 Morley, C.K., Cunningam, S.M., Wescott, W.A. and Harper, R.M., 1999. Geology and

373 geophysics of the Rukwa rift. In: *Geoscience of Rift Systems - Evolution of East Africa*

374 (C.K. Morley, ed). *AAPG Studies in Geology,* **44**, 91-110.

375 Mulibo, G.D. and Nyblade, A.A., 2013a. The P and S wave velocity structure of the mantle

376 beneath eastern Africa and the African superplume anomaly. *Geochemistry, Geophysics,*

377 *Geosystems*, **14**, 2696-2715.

378 Mulibo, G.D. and Nyblade, A.A., 2013b. Mantle transition zone thinning beneath eastern Africa:

379 Evidence for a whole-mantle superplume structure. *Geophysical Research Letters*, **40**,

380 3562-3566.

381 Nolet, G., Karato, S.I. and Montelli, R., 2006. Plume fluxes from seismic tomography. *Earth and*

382 *Planetary Science Letters*, **248**, 685-699.

383 Nyblade, A.A., Owens, T.J., Gurrola, H., Ritsema, J. and Langston, C.A., 2000. Seismic evidence

384 for a deep upper mantle thermal anomaly beneath east Africa. *Geology*, **28**, 599-602.

385 Pasteels, P., Villeneuve, M., De Paepe, P. and Klerkx, J., 1989. Timing of the volcanism of the

386 southern Kivu province: implications for the evolution of the western branch of the East

387 African Rift system. *Earth and Planetary Science Letters*, **94**, 353-363.

388 Pérez-Gussinyé, M., Metois, M., Fernández, M., Vergés, J., Fullea, J., and Lowry A.R., 2009.

389 Effective elastic thickness of Africa and its relationship to other proxies for lithospheric

390 structure and surface tectonics. *Earth and Planetary Science Letters*, **287**, 152–167.

391 Pik, R., Marty, B. and Hilton, D.R., 2006. How many mantle plumes in Africa? The geochemical

392 point of view. *Chemical Geology*, **226**, 100-114.

393   Ring, U., 1994. The influence of preexisting structure on the evolution of the Cenozoic Malawi

394   Rift (East African Rift system). *Tectonics*, **13**, 313-326.

395   Ring, U., 2014. The East African Rift System. *Austrian Journal Earth Sciences*, **107**, 132-146.

396   Ring, U., Betzler, C. and Delvaux, D., 1992. Normal vs. strike-slip faulting during rift

397   development in East Africa: the Malawi rift. *Geology*, **20**, 1015-1018.

398   Ritsema, J., Nyblade, A.A., Owens, T.J. and Langston, C.A., 1998. Upper mantle seismic

399   velocity structure beneath Tanzania, East Africa: Implications for the stability of cratonic

400   lithosphere. *Journal of Geophysical Research*, **103**, 21201-21213.

401   Ritsema, J., van Heijst, H.J. and Woodhouse, J.H., 1999. Complex shear wave velocity structure

402   imaged beneath Africa and Iceland. *Science*, **286**, 1925-1928.

403   Roberts, E.M., Stevens, N.J., O'Connor, P.M., Dirks, P.H.G.M., Gottfried, M.D., Clyde, W.C.,

404   Armstrong, R.A., Kemp, A.I.S. and Hemming, S., 2012. Initiation of the western branch

405   of the East African Rift coeval with the eastern branch. *Nature Geoscience*, **5**, 289-294.

406   Saria, E., Calais, E., Stamps, D.S., Delvaux, D. and Hartnady, C.J.H., 2014. Present-day

407   kinematics of the East African Rift. *Journal of Geophysical Research*, **119**, 3584-3600.

408   Rooney, T.O., Herzberg, C. and Bastow, I.D., 2012. Elevated mantle temperature beneath East

409   Africa. *Geology*, **40**, 27-30.

410   Sippel, J. et al., 2017. The Kenya rift revisited: insights into lithospheric strength through data-

411   driven 3-D gravity and thermal modelling. *Solid Earth*, **8**, 45.

412   Smets, B., Delvaux, D., Ross, K. A., Poppe, S., Kervyn, M., d'Oreye, N. and Kervyn, F., 2016.

413   The role of inherited crustal structures and magmatism in the development of rift

414   segments: Insights from the Kivu basin, western branch of the East African Rift.

415   *Tectonophysics*, **683**, 62-76.

416 Smith, M., 1994. Stratigraphic and structural constraints on mechanisms of active rifting in the

417   Gregory Rift, Kenya. *Tectonophysics*, **236**, 3-22.

418 Stamps, D.S., Calais, E., Saria, E., Hartnady, C., Nocquet, J.M., Ebinger, C.J. and Fernandes,

419   R.M., 2008. A kinematic model for the East African Rift. *Geophysical Research Letters*,

420   **35**.

421 Theunissen, K., Klerkx, J., Melnikov, A. and Mruma, A., 1996. Mechanisms of inheritance of rift

422   faulting in the western branch of the East African Rift, Tanzania. *Tectonics*, **15**, 776-790.

423 Versfelt, J. and Rosendahl, B.R., 1989. Relationships between pre-rift structure and rift

424   architecture in Lakes Tanganyika and Malawi, East Africa. *Nature*, **337**, 354-357.

425 Weeraratne, D.S., Forsyth, D.W., Fischer, K.M. and Nyblade, A.A., 2003. Evidence for an upper

426   mantle plume beneath the Tanzanian craton from Rayleigh wave tomography. *Journal of*

427   *Geophysical Research: Solid Earth*, **108**.

428 Wenker, S. and Beaumont, C., 2016. Effects of lateral strength contrasts and inherited

429   heterogeneities on necking and rifting of continents. *Tectonophysics*,

430   http://dx.doi.org/10.1016/j.tecto.2016.10.011.

431 Williams, L.A.J., 1982. Physical aspects of magmatism in continental rifts. *Continental and*

432   *oceanic rifts*, 193-222.

433 Zeyen, H., Volker, F., Wehrle, V., Fuchs, K., Sobolev, S.V. and Altherr, R., 1997. Styles of

434   continental rifting: crust-mantle detachment and mantle plumes. *Tectonophysics*, **278**,

435   329-352.

436

Figure captions
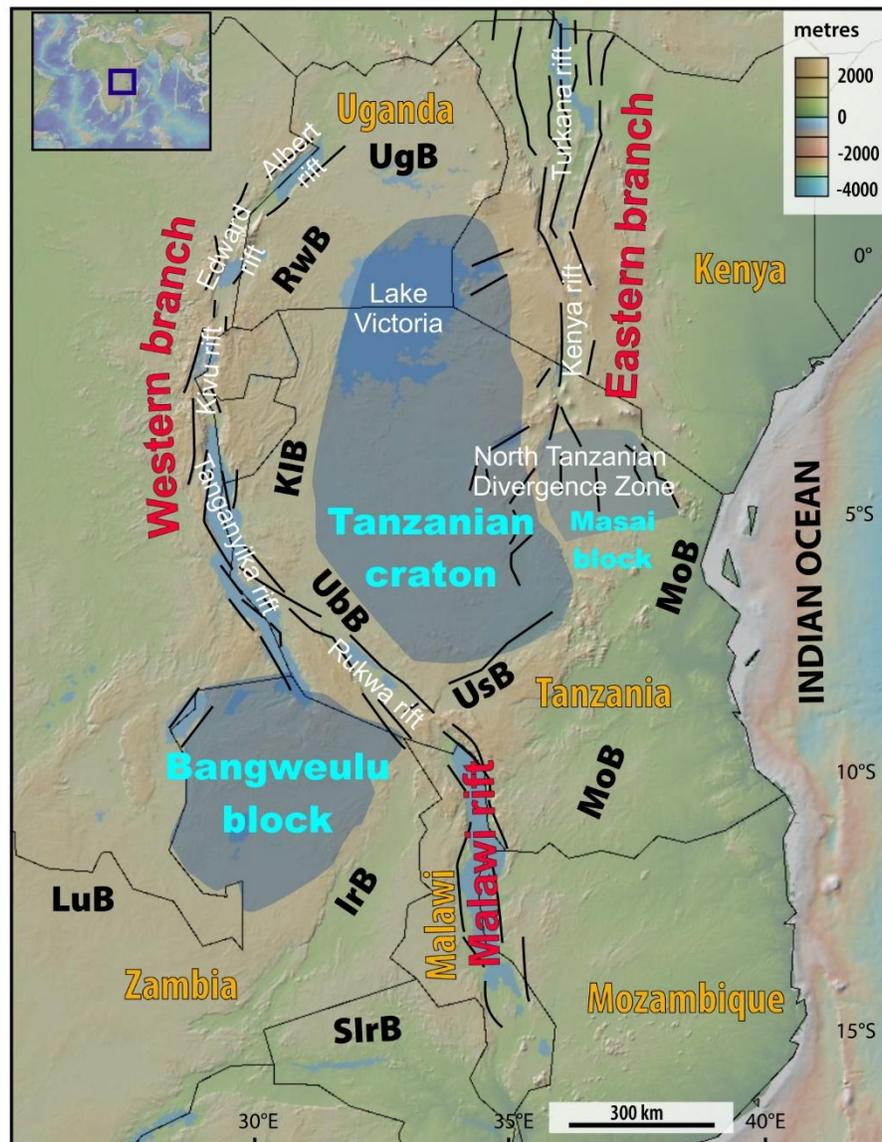
Figure 1. Topographic map showing the tectonic setting of the central and southern EARS (after
Mulibo and Nyblade (2013b) and Corti et al. (2013)) that comprises the Tanzanian craton that
likely includes the Uganda Basement Complex (UgB), the Bangweulu block, the Masai block and
several Proterozoic orogenic belts: Rwenzori (RwB), Kibaran (KiB), Ubendian (UbB), Usagaran
(UsB), Mozambique (MoB), Iruminde (IrB), Southern Iruminde (SIrB), Lufilian (LuB). Black
lines show major faults (Corti et al., 2013). The inset indicates the location of the studied area.
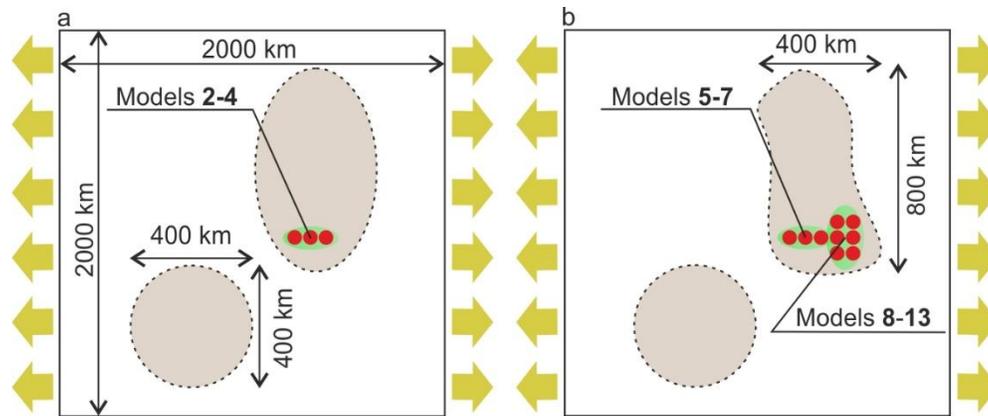
Figure 2. Model setups for the general model series shown on Figure 4: a) the models **2-4**, characterized by a simple quasi-rectangular shape of the Tanzanian craton as in previously published experiments (Koptev et al., 2015, 2016); b) the models **5-13**, with a more complex asymmetrical configuration of the Tanzanian block (based on its present-day surface outline). Initial plume positions are shown by red circles within tested areas (shaded green) with respect to cratonic blocks (gray ellipses). "No-plume" model **1** (see Figure 3) is characterized by simple symmetrical configuration of the Tanzanian craton and by absence of pre-imposed mantle plume anomaly. The initial model setup and geotherm have been adopted with respect to observation-based models of regional thermal and rheological structure of the continental lithosphere in East Africa (Artemieva et al., 2006; Albaric et al., 2009; Pérez-Gussinyé et al., 2009; Fishwick and Bastow, 2011). Rheological parameters have been chosen in consideration of extensive and successful experience obtained from heterogeneous continental rifting (e.g., Huismans and Beaumont, 2007; Wenker and Beaumont, 2016 and references therein) and plume-lithosphere interaction modelling (e.g., Burov and Guillou-Frottier, 2005; Burov et al., 2007; Burov and Cloetingh, 2010; Burov, 2011; Burov and Gerya, 2014; Koptev et al., 2017a,b; Beniest et al., 2017a,b) including our previous Africa-oriented experiments (Koptev et al., 2015, 2016) that have permitted to reproduce a number of key features of the central EARS as timing, surface velocity distribution, and large-scale topography.

1.Sym.No plume

$0 \qquad 15 \times 10^{-16} \quad 3 \times 10^{-15} [s^{-1}]$

464
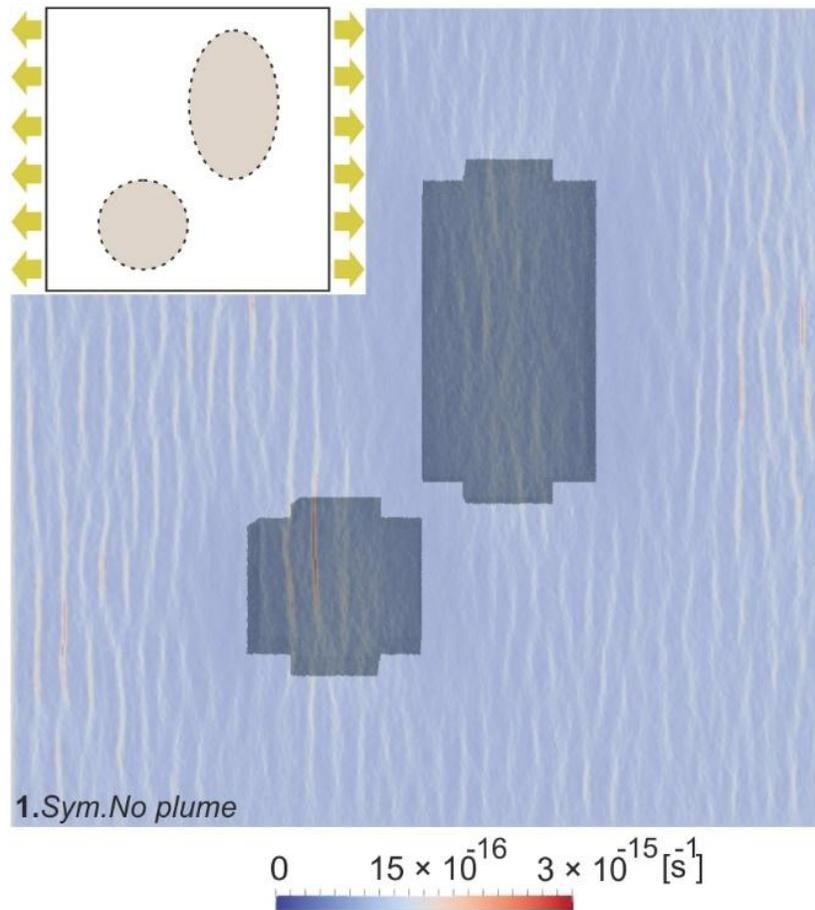
Figure 3. "No-plume" model **1** at 5 Myr. Blue to red colors indicate crustal strain rate. The cratons are the dark gray volumes. Unidirectional tectonic stretching of the continental lithosphere in the absence of active mantle upwelling results in distributed closely spaced small-offset parallel faults, which are not localized within any particular zone. Upper crustal distributed deformation covers all model domains uniformly (including the cratonic areas) because of lateral homogeneity of the crustal composition adopted in the general model series. Note that progressive focusing and amplification of localized non-axisymmetric deformation is generated only by simultaneous presence of the hot plume material underneath the lithosphere basement and passive horizontal extension while mantle plume impingement on non-pre-stressed lithosphere can only result in axisymmetric domal-shaped features with multiple radiating rifts (see Burov and Gerya, 2014 for more detail).
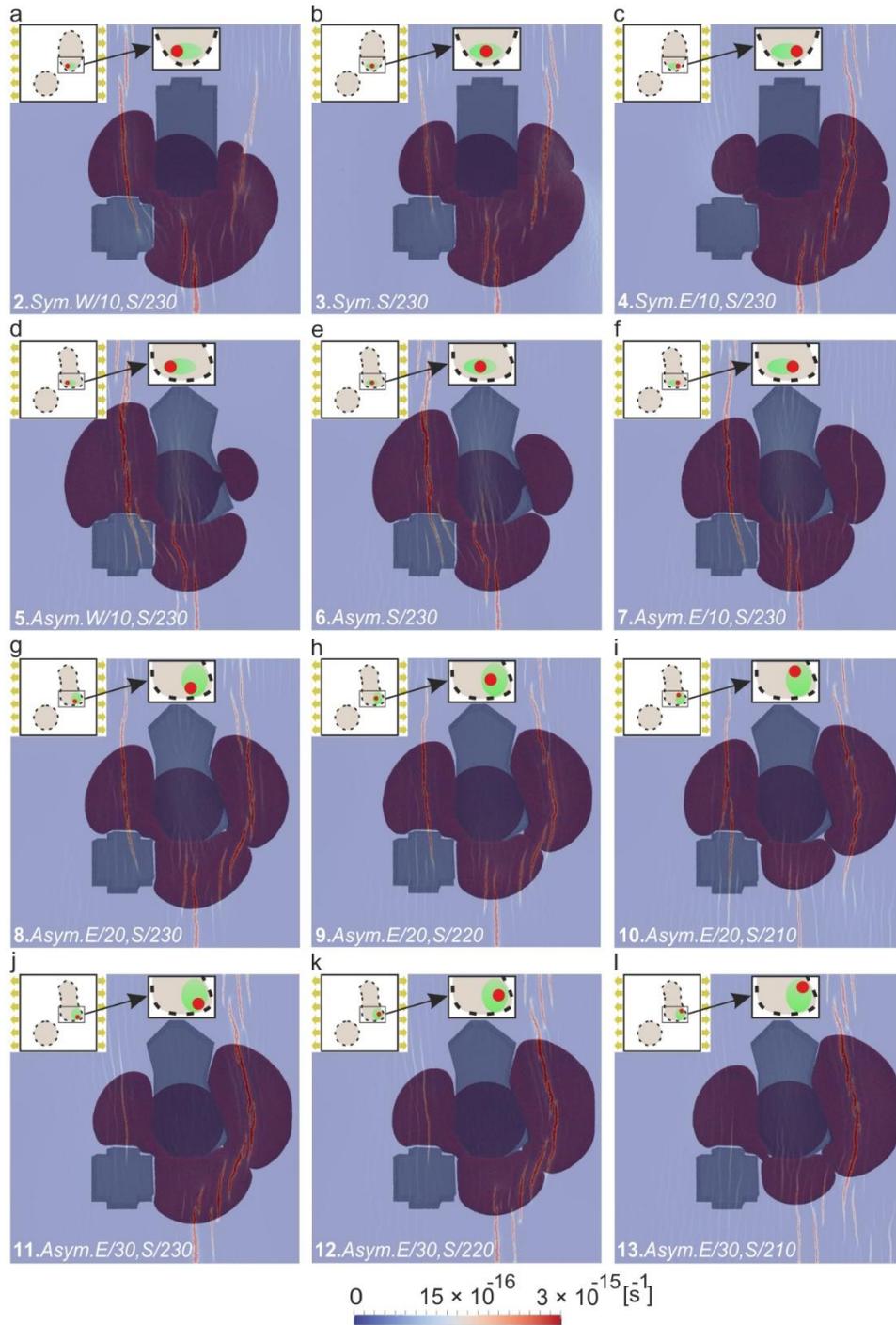
Figure 4. Top view of the results of 3D experiments **2**-**13** at 5-10 Myr. The plume material is shown in dark red. Left top insets schematically illustrate initial position of the mantle plume. Note that relative position of lithospheric heterogeneities and initial mantle plume anomaly appears to be the crucial factor for resulting rifting pattern.
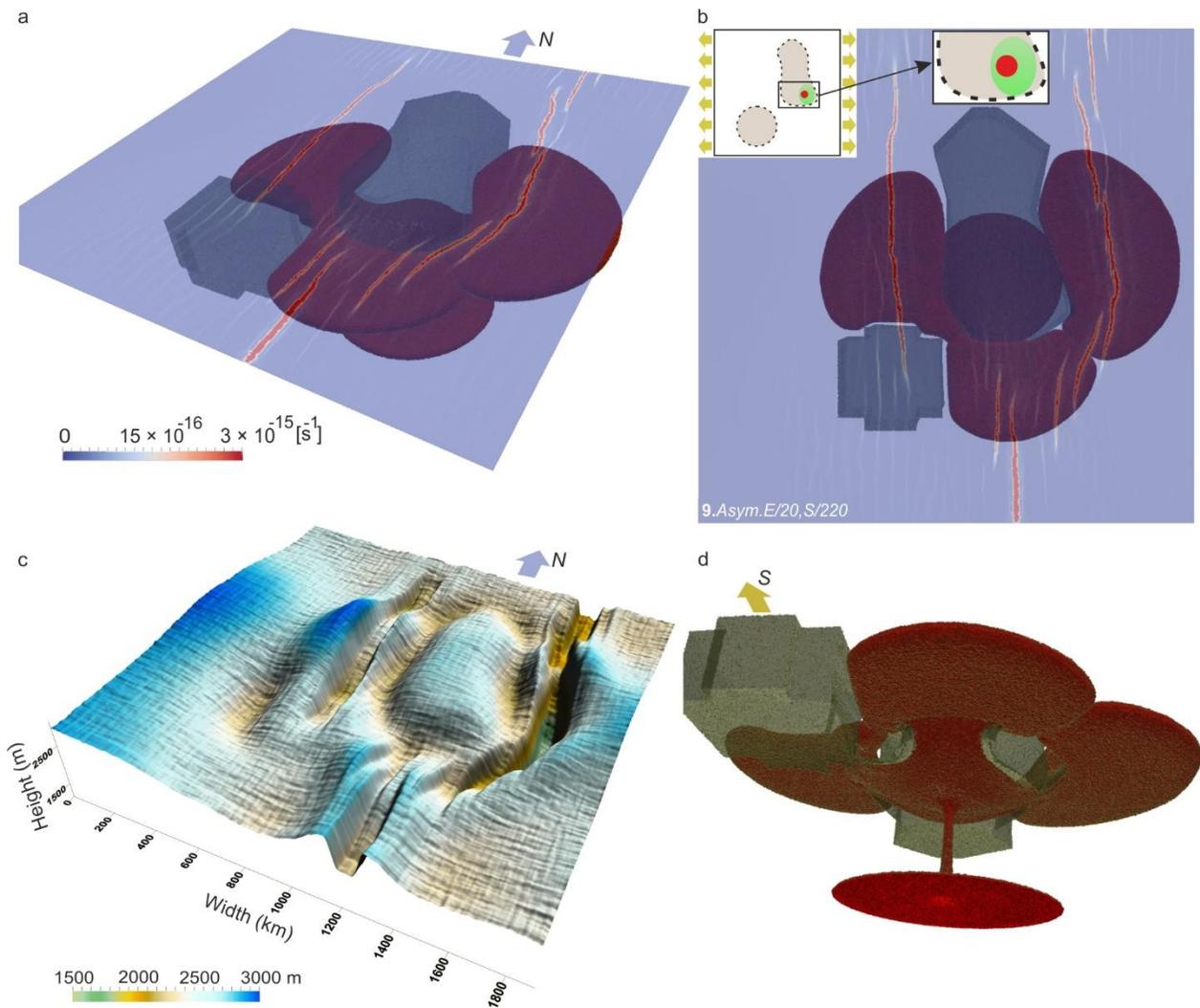
Figure 5. The "best-fit" experiment **9** (*Asym.E/20,S/220*) of the general model series: a) 3D view; b) top view; c) corresponding surface topography; d) bottom view. Note that strain distribution bears strong similarities with the central and southern EARS showing the "three-branches" pattern with simultaneous development of the Eastern branch, the Western branch and the Malawi rift.
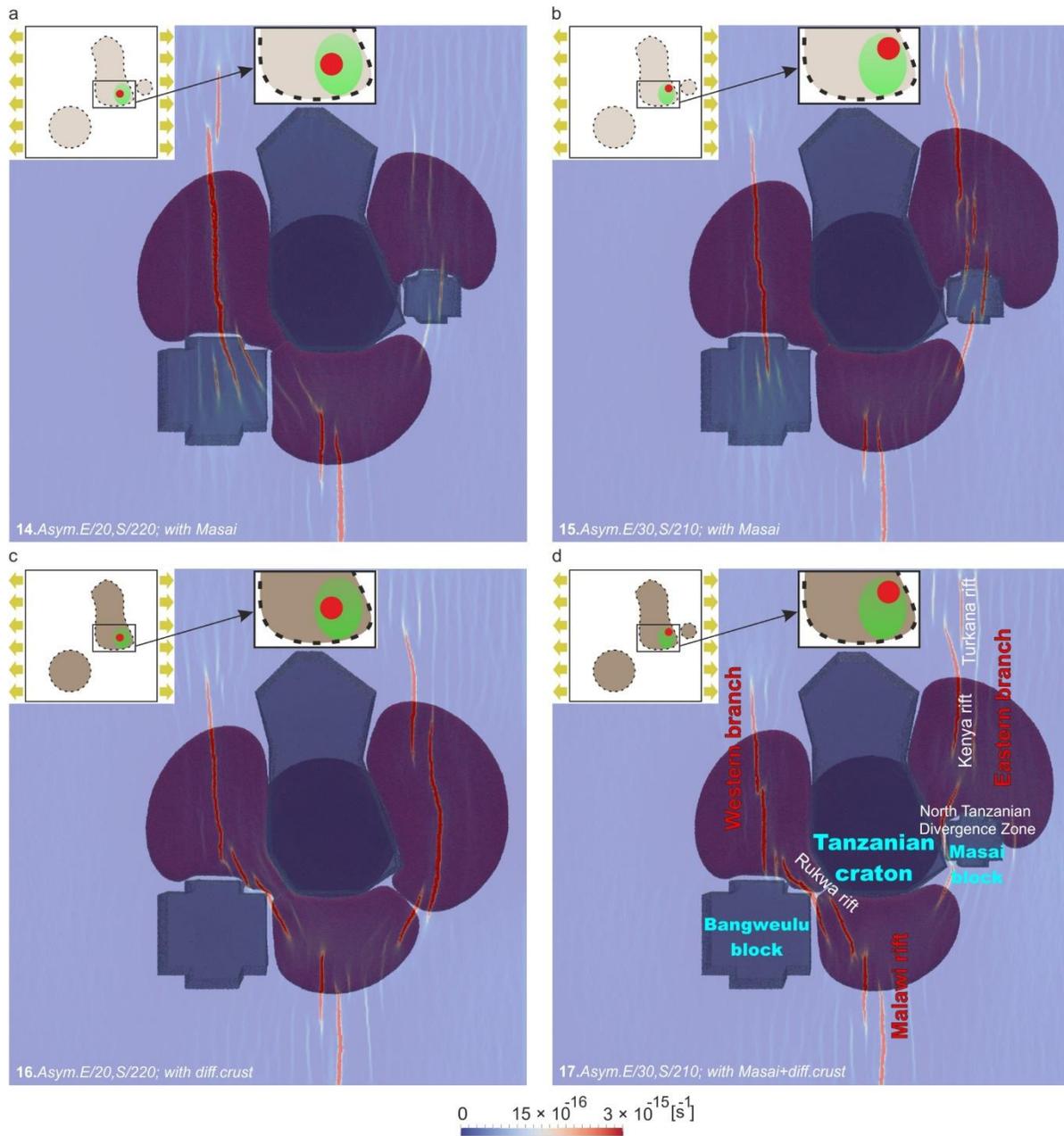
Figure 6. Top view of the complementary models **14**-**17** at 5-10 Myr. Complementary models differ from the general model series (models **1**-**13**; Figure 4-5) by: a-b, d) the presence of third area of lithospheric thickening corresponding to the Masai block (models **14**-**15**, **17**) and/or by c-d) a stronger rheology for the lower crust within cratonic areas (models **16**-**17**). Note that these experiments containing more predefined complexities provide better fitting with the observed data than in case of the general model series. In particular, the model **17** reproduces not only

494   three first-order rift structures corresponding to the Eastern branch, the Western branch and the

495   Malawi rift but also such second-order features as NW-SE oriented Rukwa rift and along-axis

496   transition observed between the narrow Kenya rift and the broader Turkana depression to the

497   north and the multi-basin North Tanzania Divergence Zone to the south (compare Figure 1 and

498   Figure 6d).

499

Table 1. Controlling parameters of the models.

Model number	Model series	Model title	Controlling parameters				Figure
			Tanzanian craton shape	Plume position (az/shift, km)	Presence of the Masai block	Stronger lower crust for cratons	
1	General	*Sym.No plume*	Symmetrical	-	No	No	Fig.3
2	General	*Sym.W/10,S/230*	Symmetrical	W/10, S/230	No	No	Fig4a
3	General	*Sym.S/230*	Symmetrical	E/0, S/230	No	No	Fig4b
4	General	*Sym.E/10,S/230*	Symmetrical	E/10, S/230	No	No	Fig4c
5	General	*Asym.W/10,S/230*	Asymmetrical	W/10, S/230	No	No	Fig4d
6	General	*Asym.S/230*	Asymmetrical	E/0, S/230	No	No	Fig4e
7	General	*Asym.E/10,S/230*	Asymmetrical	E/10, S/230	No	No	Fig4f
8	General	*Asym.E/20,S/230*	Asymmetrical	E/20, S/230	No	No	Fig4g
9	General	*Asym.E/20,S/220*	Asymmetrical	E/20, S/220	No	No	Fig4h; Fig.5
10	General	*Asym.E/20,S/210*	Asymmetrical	E/20, S/210	No	No	Fig4i
11	General	*Asym.E/30,S/230*	Asymmetrical	E/30, S/230	No	No	Fig4j
12	General	*Asym.E/30,S/220*	Asymmetrical	E/30, S/220	No	No	Fig4k
13	General	*Asym.E/30,S/210*	Asymmetrical	E/30, S/210	No	No	Fig4l
14	Complementary	*Asym.E/20,S/220; with Masai*	Asymmetrical	E/20, S/220	Yes	No	Fig6a
15	Complementary	*Asym.E/30,S/210; with Masai*	Asymmetrical	E/30, S/210	Yes	No	Fig6b
16	Complementary	*Asym.E/20,S/220; with diff.crust*	Asymmetrical	E/20, S/220	No	Yes	Fig6c
17	Complementary	*Asym.E/30,S/210; with Masai+diff.crust*	Asymmetrical	E/30, S/210	Yes	Yes	Fig6d